A General Framework for Finite Element *A Posteriori* Error Control: Application to Linear and Nonlinear Convection–Dominated Problems

Luc Machiels Anthony T. Patera Jaume Peraire
Massachusetts Institute of Technology, Cambridge, Massachusetts, USA

Yvon Maday
Laboratoire d'Analyse Numérique, Université Pierre et Marie Curie, Paris, France

1 Introduction

We consider an engineering system or component — such as a MEMS device, heat exchanger, or airframe — characterized by a design variable (or vector); the design variable may represent the geometry of the configuration, or perhaps the physical properties of the constituents. We assume that the physical behavior of the system may be adequately represented by the solution of a partial differential equation, or set of partial differential equations, describing the relevant thermal, mechanical, fluid, and electromagnetic phenomena.

A typical engineering "forward" analysis is initiated by the specification of the design variable; the partial differential equation then yields a set of field variables (such as temperature or displacement or velocity or electric field); finally, on the basis of these intermediate field variables, the output can be evaluated. Here "output" denotes the engineering quantity (or quantities) of interest, that is, the metrics relevant to the performance of the system; typical outputs are the temperature at a point in the domain, the average displacement over a boundary segment, the lift, drag, and flowrate, or the electromagnetic cross–section.

Of ultimate interest, of course, is not the forward problem, but the "design problem." In brief, the design problem articulates the engineering objectives and constraints as a function of the outputs, and then seeks the best value of the design variable with respect to the selected criteria. Successful solution of the design problem requires repeated appeal to the forward problem in order to calculate the output and the sensitivity derivatives of the output with respect to the design variables.

For most problems of engineering interest, the underlying partial differential equations are far too complex to admit analytical solution, and a numerical approximation must thus be introduced. The requirements on the numerical approximation are twofold: the approximation must be sufficiently coarse so as to permit repeated appeal within the design context; the approximation must be sufficiently fine so that the numerical prediction of the desired outputs is representative of the true performance of the system.

A posteriori error control offers great promise in reconciling these often conflicting requirements. *A posteriori* analysis [3, 20] is composed of two critical ingredients: an estimation procedure which inexpensively assesses the error in a particular numerical solution; and an adaptive refinement procedure which exploits this error information to optimally improve the numerical solution. The objectives of *a posteriori* error control are twofold: to eliminate numerical uncertainty — arguably the single largest impediment to widespread adoption of simulation–based design; and to improve numerical efficiency — thus permitting much more extensive design exploration. In fact, greater certainty is a prerequisite for greater efficiency: we may consider a less expensive (or even *the* least–expensive) discretization only if the associated error can be quantified, and hence constrained and controlled; we are no longer compelled to choose *either* certainty or efficiency — both can be achieved.

In order to clearly demonstrate the potentially large impact of error control procedures on the effectiveness of simulation–based design we present an illustrative example. We consider the Burgers equation as a model for the more complex fluid dynamics problems — the multidimensional incompressible and compressible Euler and Navier–Stokes equations — that are ultimately of interest. The field variable u thus satisfies $-\nu u_{xx} + u u_x = 0,\ u(0) = 1,\ u(1) = 0$, where $\nu = 0.04$ is the viscosity. We take as our engineering output of interest the velocity at a particular point in the domain, $\overline{x} = 0.875$; other possible engineering outputs include, for example, the "stress" at $x = 1$, $\nu u_x(1)$.

We first demonstrate the unsatisfactory state of affairs in the case in which we do not evoke *a posteriori* error analysis. We would clearly prefer to consider a rather coarse — and hence very inexpensive — finite element mesh comprising (say) 8 elements of length $H = 1/8$. However, there is no way to estimate *a priori* the error in the velocity at $\overline{x}$ on this mesh, and thus the predictions are of very limited value. We will thus most likely resort to an extremely fine mesh — comprising (say) $8,192$ elements of length $h = 1/8192$ — which rather patently, indeed excessively, resolves the relevant physical length scales, and which should thus provide predictions which are arbitrarily close to the true result. Unfortunately, the calculations on this very fine mesh will be inordinately expensive. In short, because of the absence of precise error control, we are forced to choose between fidelity and efficiency. (Note that, as regards computational efficiency, our remarks anticipate the treatment of problems in higher space dimensions.)

A posteriori analysis resolves this conflict by allowing us to consider a relatively coarse mesh while *still maintaining quantitative control over the accuracy of the output of interest*: "overkill" is no longer required. In particular, our *a posteriori* error analysis procedure permits us to compute — very inexpensively — that the velocity at $\overline{x}$ predicted by the coarse mesh ($H = 1/8$) is, in fact, within 30.8% of the exact result (or, more precisely, the "effectively exact" result predicted by the fine mesh, $h = 1/8192$); if this error in the coarse–mesh output is deemed sufficiently small, the predictions can be safely accepted. It is important to emphasize that, even in the absence of adaptive refinement, error estimation leads not only to greater certainty, but also to greater computational efficiency: we can consider a coarse mesh only because we can verify the accuracy of the resulting prediction — by definition, "marginal" resolution is optimal.

In the case in which the 30.8% accuracy afforded by the coarse mesh is not adequate, we can exploit our error bounds — appropriately decomposed into elemental contributions — to guide the subsequent refinement process. For example, if we set our relative error tolerance at 0.1%, we arrive after several refinement levels at a non–uniform mesh of 36 elements — on which we are ensured that the error in the velocity at $\overline{x}$ is no larger than 0.1%. We note that the computations on this optimal mesh are not only inexpensive compared to the very fine mesh ($h = 1/8192$) — which is the essential advantage of *a posteriori* error estimation — but also considerably less expensive than computations on a uniformly refined mesh of commensurate accuracy — which is the essential advantage of adaptive refinement. In some sense, *a posteriori* error control is a synthesis of discretization and solution methods: inexpensive inversion of an inexpensive approximation.

We close this example by noting that, if we exhaust our computational resources before our error tolerance is satisfied, we must simply conclude that our accuracy and efficiency constraints are incompatible. We contend that this "negative" result is, in fact, far better than the acceptance of incorrect information that could seriously mislead the design process. Nevertheless, we must make sure to minimize false negatives — the error bounds must be sufficiently accurate.

It should be clear that the crucial "enabling technology" in this example is the ability to obtain inexpensive, sharp, rigorous, and quantitative ("constant–free") *bounds* for the numerical error in the *engineering outputs of interest*; in this regard our method [13, 15, 18, 11] represents a significant advance over alternative error control proposals. In particular, in all earlier *a posteriori* error analysis techniques, either — in implicit approaches — the measure of the error is *not related to the actual engineering outputs of interest* (e.g., [9, 4, 2]), or — in explicit approaches — the error estimates for the engineering outputs of interest involve *numerous undetermined or uncertain constants or functions* (e.g., [5, 6, 19]); in both cases, quantitative confirmation — and hence both certainty and efficiency — is seriously compromised, and the relevance to engineering design greatly reduced.

Although our method provides a critical new capability, we are nevertheless indebted to earlier *a posteriori* implicit (Neumann subproblem) techniques [9, 4, 2] for several important conceptual and mathematical ingredients — in particular duality theory and flux "hybridization." The former, though not strictly "necessary," provides a derivational mechanism without which the requisite equations are very difficult to motivate; the latter — technically quite subtle — is the crucial component in ensuring computational efficiency. Our framework may thus be viewed as a generalization of earlier implicit techniques [2]; equivalently, these earlier techniques can be interpreted as special cases of our new formulation. We give in [18] a more detailed comparison between our approach and earlier implicit (and explicit) *a posteriori* error control proposals.

Our initial formulation [15, 18] focused on symmetric coercive problems (e.g., Poisson and Linear Elasticity), and nonsymmetric coercive problems (e.g., Convection–Diffusion), as well as certain constrained problems (the Stokes equations, central to hydrodynamics [14]). However, we have recently developed a more general formulation [17, 10] that greatly expands the class of equations and outputs that may be treated; in particular, noncoercive problems (e.g., the Helmholtz equation [17, 10]), nonlinear problems (e.g., the Burgers equation [17, 10], the eigenvalue problem [10]), and nonlinear outputs can now be addressed. In this paper we shall focus on linear (stabilized) and nonlinear convection–dominated problems.

2 General Formulation

We consider here a generalization of the formulation given in [10] which permits us to address stabilized schemes and, more generally, variational crimes.

2.1 Definitions

We consider the problem of finding $u \in Y$ such that

$$\mathcal{A}(u, v) = 0, \quad \forall v \in Y, \tag{2.1}$$

where Y is an appropriate function space defined over a domain Ω with boundary $\partial\Omega$, and $\mathcal{A} : Y \times Y \to I\!R$ is a general form linear in the second argument. For simplicity we consider only homogeneous essential boundary conditions; the extension to the inhomogeneous and natural cases is simple, and will be discussed in the examples of Section 3. We denote the output of interest by $s = \mathcal{S}(u)$, where $\mathcal{S} : Y \to I\!R$ is a continuous functional.

We next assume that we are given two finite element approximation subspaces: Y_H, the coarse space, and Y_h, the fine space; we require that $Y_H \subset Y_h \subset Y$. The associated coarse–space (u_H) and fine–space (u_h) field variable approximations satisfy

$$\mathcal{A}_H(u_H, v) = 0, \quad \forall v \in Y_H, \tag{2.2}$$

and

$$\mathcal{A}_h(u_h, v) = 0, \quad \forall v \in Y_h, \tag{2.3}$$

respectively; the corresponding coarse–mesh and fine–mesh outputs are then given by $s_H := \mathcal{S}(u_H)$ and $s_h := \mathcal{S}(u_h)$. Note that, with the introdution of an appropriate basis, (2.2) and (2.3) produce algebraic systems of size the dimension of Y_H and Y_h, respectively.

Our assumption is that Y_H is any proposed mesh, but that Y_h is sufficiently fine that $\mathcal{S}(u_h)$ is indistinguishable from $\mathcal{S}(u)$. In our examples, Y_H will be the space of continuous piecewise–linear polynomials over a triangulation $\mathcal{T}_H$, while Y_h will be the space of continuous piecewise–linear polynomials over a much finer triangulation $\mathcal{T}_h$; members of both Y_H and Y_h must vanish on $\partial\Omega$. We shall denote the characteristic mesh sizes (triangulation diameters) associated with $\mathcal{T}_H$ and $\mathcal{T}_h$ as H and h, respectively. Note that the forms $\mathcal{A}_H$ and $\mathcal{A}_h$ need not coincide with $\mathcal{A}$: of particular interest here will be the case in which $\mathcal{A}_H$ and $\mathcal{A}_h$ contain stabilization terms which depend on the characteristic mesh size; consistency will, of course, require that $\mathcal{A}_H$ and $\mathcal{A}_h$ approach $\mathcal{A}$ as $H, h \to 0$.

2.2 Estimator Procedure

Before we can describe the bound procedure we require a few additional definitions. First, we define $\mathcal{E}(w, v) := \mathcal{A}_h(u_H + w, v) - \mathcal{A}_h(u_H, v)$, and note that

$$\mathcal{E}(e, v) = R^u(v), \quad \forall v \in Y_h, \tag{2.4}$$

where $e := u_h - u_H \in Y_h$ is the error in the field variable, and $R^u(v) = -\mathcal{A}_h(u_H, v)$ is the residual; equation (2.4) is central to all *a posteriori* approaches.

We then expand the form $\mathcal{E}$ as

$$\mathcal{E}(w, v) = E(w, v) + F(w, w, v) + G(w, v), \tag{2.5}$$

where E, F, and G represent respectively the bilinear, trilinear, and higher–order contributions; note that F is symmetric in the first two arguments. We shall denote the symmetric part of E by E^s; in many cases it will be advantageous to decompose E^s as $E^s = E^s_Y + E^s_0$, and to further define $E^s_\gamma = E^s_Y + \gamma E^s_0$ for γ a real parameter (typically zero or unity).

We also represent our output functional as an appropriate "Taylor" series about u_H,

$$\mathcal{S}(u_H + w) = \mathcal{S}(u_H) + L(w) + M(w, w) + N(w), \tag{2.6}$$

where L, M, and N are the linear, bilinear, and higher–order contributions, respectively; note the M is a symmetric bilinear form. For a linear output functional $M = N = 0$.

Lastly, we require broken spaces $\hat{Y}_H \subset \hat{Y}_h$ such that, for $\delta = h$ or H,

$$Y_\delta = \{v \in \hat{Y}_\delta \mid b_\delta(v, q) = 0, \forall q \in Q\}, \tag{2.7}$$

where Q is a Hilbert space (with associated approximation subspace Q_H) and $b_\delta : \hat{Y}_h \times Q \to I\!R$ is a bilinear form. For our purposes here, $\hat{Y}_H$ and $\hat{Y}_h$ are identical to Y_H and Y_h, respectively, save that member functions need no longer (i) vanish on $\partial\Omega$, or (ii) be continuous over the edges of the elements (triangles) in $\mathcal{T}_H$; note that functions in $\hat{Y}_h$ *are* continuous over edges of $\mathcal{T}_h$ *interior* to the triangles of $\mathcal{T}_H$. In essence, to obtain $\hat{Y}_H$ and $\hat{Y}_h$ we pull Y_H and Y_h apart at the "seams" defined by the edges of $\mathcal{T}_H$ — in short, a domain decomposition prescribed by the coarse triangulation. The spaces Q and Q_H are then defined over the edges of $\mathcal{T}_H$: Q includes all square integrable functions; members of Q_H are linear on each edge [9, 4, 2]. Finally, the bilinear form b_δ is a weighted sum of the integrals over each edge of $\mathcal{T}_H$ of the product of q and the *jump* in v (trace of v on $\partial\Omega$); the condition (2.7) is thus satisfied, since $b_\delta(v,q) = 0,\ \forall q \in Q$, forces the jumps in v (and trace of v on $\partial\Omega$) to vanish, thus re–imposing the necessary continuity and boundary conditions.

The estimator procedure takes as inputs (i) the coarse–mesh approximation u_H of (2.2), (ii) a coarse–mesh adjoint $\psi_H \in Y_H$, and (iii) "hybrid fluxes" $p_H^u \in Q_H$ and $p_H^\psi \in Q_H$; the construction of appropriate ψ_H and (p_H^u, p_H^ψ) will be discussed shortly. We then compute the reconstructed errors $\hat{e}_\pm^u, \hat{e}_\pm^\psi \in \hat{Y}_h$ according to

$$2\mathcal{H}^\pm_{\alpha\beta\gamma}(\hat{e}^u_\pm, v) - R^u(v) + b_h(v, p_H^u) = 0, \quad \forall v \in \hat{Y}_h, \tag{2.8a}$$

$$2\mathcal{H}^\pm_{\alpha\beta\gamma}(\hat{e}^\psi_\pm, v) - R^\psi(v) + b_h(v, p_H^\psi) = 0, \quad \forall v \in \hat{Y}_h. \tag{2.8b}$$

Here

$$R^\psi(v) := -L(v) - E(v, \psi_H), \tag{2.9}$$

and $\mathcal{H}^\pm_{\alpha\beta\gamma} : \hat{Y}_h \times \hat{Y}_h \to I\!R$ is the symmetric bilinear form given by

$$\mathcal{H}^\pm_{\alpha\beta\gamma}(w, v) := E^s_\gamma(w, v) \mp \alpha M(w, v) \mp \beta F(w, v, \psi_H), \tag{2.10}$$

where α and β are real parameters. Finally, we compute the lower and upper estimators,

$$s_- := \mathcal{S}(u_H) - \kappa_L \mathcal{H}^-_{\alpha\beta\gamma}(\hat{e}^{\kappa_L}_-, \hat{e}^{\kappa_L}_-) - R^u(\psi_H), \tag{2.11a}$$

$$s_+ := \mathcal{S}(u_H) + \kappa_U \mathcal{H}^+_{\alpha\beta\gamma}(\hat{e}^{\kappa_U}_+, \hat{e}^{\kappa_U}_+) - R^u(\psi_H), \tag{2.11b}$$

where $\hat{e}^{\kappa_L}_- = \hat{e}^u_- + \frac{1}{\kappa_L}\hat{e}^\psi_-$ and $\hat{e}^{\kappa_U}_+ = \hat{e}^u_+ - \frac{1}{\kappa_U}\hat{e}^\psi_+$ for $\kappa_L,\ \kappa_U \in I\!R_+$. Note that we can view $\hat{u}^L_h := u_H + \hat{e}^{\kappa_L}_-$ and $\hat{u}^U_h := u_H + \hat{e}^{\kappa_U}_+$ as *a posteriori* fine–mesh reconstructed solutions.

As we will see shortly, the lower and upper estimators are, in fact, lower and upper *bounds* for $\mathcal{S}(u_h)$, the effectively exact output on the fine mesh. Clearly, once we obtain these bounds, we can also bound the *error* in $\mathcal{S}(u_H)$, which is the usual approach to error estimation. We adopt a slightly different procedure: we define a *bound average*, $s_{pre} := \frac{1}{2}(s_+ + s_-)$, which thus satisfies $|s_{pre} - \mathcal{S}(u_h)| \le \Delta$, where Δ is the *bound gap*, $\Delta := \frac{1}{2}(s_+ - s_-)$; we prefer the bound average to $\mathcal{S}(u_H)$ because the uncertainty in the former is slightly reduced relative to the latter. (In fact, in our Burgers example of Section 1, it is the error in the bound average that we report.) Perhaps more importantly, we note that, from an engineering perspective, it is neither s_{pre} nor $\mathcal{S}(u_H)$ that is of the greatest utility; rather, the lower and upper bounds themselves convey the most information about the true system performance.

2.3 Estimator Properties

We must now establish several characteristics of these estimators: (i) the estimators correspond to bounds under appropriate hypotheses; (ii) the estimators are inexpensive to compute relative to $\mathcal{S}(u_h)$; (iii) the estimators converge to the true result $\mathcal{S}(u_h)$ at the optimal rate; and (iv) the estimators can provide guidance for local adaptive refinement strategies.

2.3.1 Bounding Properties

In order to show that the estimators (2.11) are (asymptotically) lower and upper bounds for $\mathcal{S}(u_h)$ — the output on the fine mesh — we first choose $v = e$ in (2.8) and sum appropriately to obtain

$$2\kappa_L \mathcal{H}^-_{\alpha\beta\gamma}(\hat{e}^{\kappa_L}_-, e) - \kappa_L R^u(e) - R^\psi(e) = 0, \tag{2.12a}$$

$$2\kappa_U \mathcal{H}^+_{\alpha\beta\gamma}(\hat{e}_+^{\kappa_U}, e) - \kappa_U R^u(e) + R^\psi(e) = 0; \tag{2.12b}$$

note that $b_h(p_H^u, e) = b_h(p_H^\psi, e) = 0$ since $e \in Y_h$. We then evoke (2.4) with $v = e$, (2.4) with $v = \psi_H$, and (2.9), to obtain

$$2\kappa_L \mathcal{H}^-_{\alpha\beta\gamma}(\hat{e}_-^{\kappa_L}, e) - \kappa_L \mathcal{E}(e,e) + L(e) - F(e,e,\psi_H) - G(e,\psi_H) + R^u(\psi_H) = 0, \tag{2.13a}$$

$$2\kappa_U \mathcal{H}^+_{\alpha\beta\gamma}(\hat{e}_+^{\kappa_U}, e) - \kappa_U \mathcal{E}(e,e) - L(e) + F(e,e,\psi_H) + G(e,\psi_H) - R^u(\psi_H) = 0. \tag{2.13b}$$

Finally, combining these last equations with (2.11) yields

$$\begin{aligned} s_- = {} & \mathcal{S}(u_h) - \kappa_L E_Y^s(e - \hat{e}_-^{\kappa_L}, e - \hat{e}_-^{\kappa_L}) \\ & -\kappa_L \gamma E_0^s(e - \hat{e}_-^{\kappa_L}, e - \hat{e}_-^{\kappa_L}) - \kappa_L \alpha M(e - \hat{e}_-^{\kappa_L}, e - \hat{e}_-^{\kappa_L}) - \kappa_L \beta F(e - \hat{e}_-^{\kappa_L}, e - \hat{e}_-^{\kappa_L}, \psi_H) \\ & -\kappa_L (1-\gamma) E_0^s(e,e) - (1 - \kappa_L \beta) F(e,e,\psi_H) - \kappa_L [F(e,e,e) + G(e,e)] \\ & -(1-\kappa_L\alpha) M(e,e) - N(e) - G(e,\psi_H), \end{aligned} \tag{2.14a}$$

$$\begin{aligned} s_+ = {} & \mathcal{S}(u_h) + \kappa_U E_Y^s(e - \hat{e}_+^{\kappa_U}, e - \hat{e}_+^{\kappa_U}) \\ & +\kappa_U \gamma E_0^s(e - \hat{e}_+^{\kappa_U}, e - \hat{e}_+^{\kappa_U}) - \kappa_U \alpha M(e - \hat{e}_+^{\kappa_U}, e - \hat{e}_+^{\kappa_U}) - \kappa_U \beta F(e - \hat{e}_+^{\kappa_U}, e - \hat{e}_+^{\kappa_U}, \psi_H) \\ & +\kappa_U (1-\gamma) E_0^s(e,e) - (1 - \kappa_U \beta) F(e,e,\psi_H) + \kappa_U [F(e,e,e) + G(e,e)] \\ & -(1-\kappa_U\alpha) M(e,e) - N(e) - G(e,\psi_H). \end{aligned} \tag{2.14b}$$

Note that $\mathcal{S}(u_h)$, the true result, not $\mathcal{S}(u_H)$, appears in (2.14).

The essential point (say for the lower estimator s_-) is that, for a large and important class of problems — semi–linear elliptic partial differential equations — there exists an E_Y^s, E_0^s splitting such that (i) E_Y^s is positive definite, and (ii) $E_Y^s(e - \hat{e}_-^{\kappa_L}, e - \hat{e}_-^{\kappa_L})$ dominates all other deviations of s_- from $\mathcal{S}(u_h)$ for H sufficiently small; we conclude that s_- approaches $\mathcal{S}(u_h)$ from below, and we thus obtain *asymptotic bounds*, as desired. In brief, (i) follows because of ellipticity, and (ii) follows because, relative to the $E_Y^s(e - \hat{e}_-^{\kappa_L}, e - \hat{e}_-^{\kappa_L})$ term, the "other corrections" — the second, third, and fourth lines of (2.14a) — involve either *weaker norms* or *higher powers* of the errors $e = u_h - u_H$ and $e - \hat{e}_-^{\kappa_L} = u_h - \hat{u}_h^L$. An analogous argument applies to the upper estimator — s_+ approaches $\mathcal{S}(u_h)$ from above for H sufficiently small. Note that for linear coercive problems only the first lines of (2.14a) and (2.14b) survive, and we thus obtain bounds for *all* H.

2.3.2 Computational Expense

We recall that u_h and $\mathcal{S}(u_h)$ are the field variable and output that are effectively indistinguishable from the truth — and correspondingly expensive. Our lower and upper bounds are only interesting if they can be obtained at considerably less expense than computation of $\mathcal{S}(u_h)$ — and preferrably at only slightly greater expense than computation of $\mathcal{S}(u_H)$, our coarse approximation. We now show that this is the case.

In particular, we see from the definitions of Y_h and the broken space $\hat{Y}_h$ that, whereas (2.3) corresponds to a single, large, global, coupled problem, (2.8) corresponds to many, local, uncoupled, smaller problems — Neumann subproblems [9, 4, 2]; it follows from the superlinearity of most general solution strategies that $\hat{e}_-^{\kappa_L}$ and $\hat{e}_+^{\kappa_U}$ will be much less expensive to compute than u_h (and hence $\mathcal{S}(u_h)$). To make this point more quantitatively, we consider banded LU decomposition, which in two space dimensions is a respectable if not optimal solution strategy. For purposes of simplicity, we consider a uniform mesh on $\Omega = [0,1]^2$, for which $\mathcal{T}_H$ and $\mathcal{T}_h$ comprise $2(1/H)(1/H)$ and $2(1/h)(1/h)$ elements, respectively. It then follows from the usual complexity arguments that (say for the lower bound) $\mathcal{W}(\hat{e}_-^{\kappa_L})/\mathcal{W}(u_h) \approx O(H^2)$ and $\mathcal{W}(\hat{e}_-^{\kappa_L})/\mathcal{W}(u_H) \approx O(H^6/h^4)$, where $\mathcal{W}(\,)$ denotes number of operations. It follows from the former that $\hat{e}_-^{\kappa_L}$ is *much less expensive* to compute than u_h; it follows from the latter that $\hat{e}_-^{\kappa_L}$ will typically be no more expensive to compute than u_H — the *coarse* approximation.

Finally, we note that there are several other factors that further significantly decrease the cost of $\hat{e}_-^{\kappa_L}$ and $\hat{e}_+^{\kappa_U}$ relative to u_h: the equations for $\hat{e}_-^{\kappa_L}$ and $\hat{e}_+^{\kappa_U}$ will be symmetric and linear (and for $\alpha = \beta = \gamma = 0$, positive definite) even when $\mathcal{A}$ enjoys none of these properties; and the equation for $\hat{e}_-^{\kappa_L}$ and $\hat{e}_+^{\kappa_U}$ admit obvious — communication–free, completely concurrent — medium–grained parallelism.

2.3.3 Estimator Accuracy

As indicated in the example of Section 1, we require not only that our estimators enjoy certain bounding properties — for certainty — but also that the bounds be sufficiently accurate that "false negatives" are rare. In particular, we do not want to reject predictions — $\mathcal{S}(u_H)$ or s_{pre} — which are, in fact, sufficiently accurate; equivalently, since the work to compute the bounds scales as the work to compute $\mathcal{S}(u_H)$, the bounds should converge to $\mathcal{S}(u_h)$ at the same rate as $\mathcal{S}(u_H)$.

The argument for optimal convergence can be made at a fairly general level. In particular, it can be shown [13, 15, 16] that our bound procedure corresponds to the application of classical duality theory to an appropriately constructed Lagrangian $\mathcal{L}_h$ for which the saddle value is the desired true output, $\mathcal{S}(u_h)$. (Strictly speaking, this applies only to linear coercive problems; for other problems we must restrict the space of admissible candidates to a cone over which the indefinite terms in (2.14) are subdominant.) We should thus choose Lagrange multipliers — in fact the adjoint and hybrid fluxes — to correspond to the saddlepoint of a Lagrangian $\mathcal{L}_H$ which evaluates to the output on the coarse mesh, $\mathcal{S}(u_H)$. For this choice of adjoint and hybrid fluxes, the precise equations for which will be given shortly, it is clear that as H approaches h, the bounds will approach the true result; and it is certainly plausible, given the usual stationarity arguments, that the bounds should approach $\mathcal{S}(u_h)$ rather rapidly. For elliptic problems [11], it can be shown that the bounds do indeed converge to $\mathcal{S}(u_h)$ at the same rate as $\mathcal{S}(u_H)$ approaches $\mathcal{S}(u_h)$; for linear elements, both converge as $O(H^2)$, as would be expected from classical Aubin–Nitsche arguments.

Finally, we note that, although we almost always obtain the optimal convergence *rate*, typically the bounds are not as accurate as $\mathcal{S}(u_H)$ — the "effectivity" is not unity. This is perhaps not surprising, since the bounds carry a direction and certainty — and hence arguably a safety margin — not present in $\mathcal{S}(u_H)$. We remark that the bound "constants" can be considerably improved by optimization over κ_L and κ_U. To wit, since we obtain (asymptotic) bounds for any real positive κ_L (respectively κ_U), we can obtain optimal bounds by maximizing (respectively minimizing) our lower (respectively upper) estimator over all admissible κ_L (respectively κ_U). This optimization can be done analytically, giving for the optimal values

$$\kappa_L = \kappa_L^* := \sqrt{\mathcal{H}^-_{\alpha\beta\gamma}(\hat{e}_-^{\psi}, \hat{e}_-^{\psi})/\mathcal{H}^-_{\alpha\beta\gamma}(\hat{e}_-^{u}, \hat{e}_-^{u})}, \tag{2.15a}$$

$$\kappa_U = \kappa_U^* := \sqrt{\mathcal{H}^+_{\alpha\beta\gamma}(\hat{e}_+^{\psi}, \hat{e}_+^{\psi})/\mathcal{H}^+_{\alpha\beta\gamma}(\hat{e}_+^{u}, \hat{e}_+^{u})}; \tag{2.15b}$$

note that, at least for $\alpha = \beta = \gamma = 0$, we are guaranteed that the arguments of the radicals are positive. The bounds then become

$$s_- := \mathcal{S}(u_H) - 2\mathcal{H}^-_{\alpha\beta\gamma}(\hat{e}^u_-, \hat{e}^\psi_-) - 2\sqrt{\mathcal{H}^-_{\alpha\beta\gamma}(\hat{e}^u_-, \hat{e}^u_-)\mathcal{H}^-_{\alpha\beta\gamma}(\hat{e}^\psi_-, \hat{e}^\psi_-)} - R^u(\psi_H), \tag{2.16a}$$

$$s_+ := \mathcal{S}(u_H) - 2\mathcal{H}^+_{\alpha\beta\gamma}(\hat{e}^u_+, \hat{e}^\psi_+) + 2\sqrt{\mathcal{H}^+_{\alpha\beta\gamma}(\hat{e}^u_+, \hat{e}^u_+)\mathcal{H}^+_{\alpha\beta\gamma}(\hat{e}^\psi_+, \hat{e}^\psi_+)} - R^u(\psi_H). \tag{2.16b}$$

This optimization is particularly important if we broaden our class of outputs to include functionals which are not continuous over Y [12] — for example, point values in $I\!R^2$. (Note that certain ostensibly unbounded functionals, such as the flux over part of the boundary, can often be expressed as equivalent bounded functions, with a corresponding increase in accuracy [12].)

2.3.4 Adaptive Refinement

As indicated in Section 1, *a posteriori* error control should be able not only to ascertain, or bound, the error in a particular output, but also to guide the subsequent approximation refinement (or de-refinement) process towards the least expensive discretization that achieves the requisite accuracy. In most *a posteriori* techniques the necessary information is obtained by re-interpreting a global error measure in terms of local, elemental contributions. Our procedure admits a similar approach; in particular, the bound gap

$$\Delta := \frac{1}{2}(s_+ - s_-) = \frac{1}{2}(\kappa_U \mathcal{H}^+_{\alpha\beta\gamma}(\hat{e}^{\kappa_U}_+, \hat{e}^{\kappa_U}_+) + \kappa_L \mathcal{H}^-_{\alpha\beta\gamma}(\hat{e}^{\kappa_L}_-, \hat{e}^{\kappa_L}_-)) \tag{2.17}$$

can be readily recast as a sum of elemental contributions. Although in general one might be forced to consider absolute values — with a corresponding decrease in sharpness — for linear coercive problems the *local* bound gaps will always be positive; furthermore, for the choice $\alpha = \beta = \gamma = 0$ the local bound gaps will be positive for *any* elliptic equation. Once local indicators are available, several different refinement strategies and implementations are possible; to date we have pursued rather standard techniques — "thresholding" for element selection and "hanging nodes" and Lagrange multipliers for mesh compatibility [18].

Note that, although the primary purpose of adaptive refinement is greater efficiency, refinement also promotes greater certainty. In particular, in those cases in which we only obtain bounds asymptotically, adaptive refinement drives the discretization to a lower error — and hence the limit in which the indefinite terms will be negligible in (2.14a) and (2.14b).

3 Application to Convection–Dominated Problems

3.1 Stabilized Linear Convection Equation

3.1.1 Formulation

We consider the stationary linear convection problem

$$\mathbf{U} \cdot \nabla u + \sigma u = f \quad \text{in } \Omega, \tag{3.1a}$$

$$u = g \quad \text{on } \partial\Omega_i, \tag{3.1b}$$

where Ω is a bounded domain in $I\!R^d$ $(d = 1, 2)$ with boundary $\partial\Omega$, σ is a real non–negative parameter, and $\mathbf{U} = (U_1, \ldots, U_d)$ is an incompressible prescribed velocity field. The boundary $\partial\Omega$ is decomposed into an inflow boundary $\partial\Omega_i := \{\mathbf{x} \in \partial\Omega \mid \mathbf{n} \cdot \mathbf{U} < 0\}$ and an outflow boundary $\partial\Omega_o = \partial\Omega \backslash \partial\Omega_i$, where $\mathbf{n}$ is the unit outward normal on $\partial\Omega$. We assume that f and g are sufficiently regular so that the problem (3.1) is well posed.

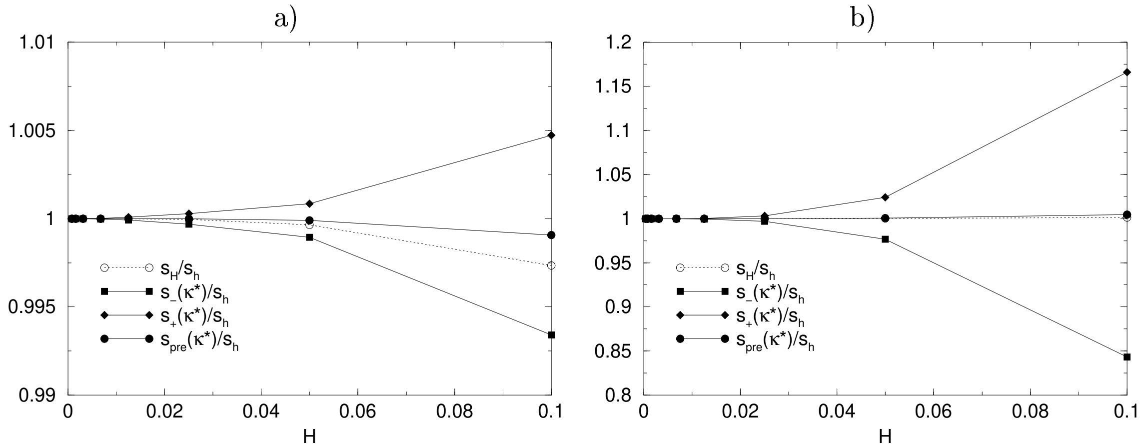

Figure 1: One–dimensional linear convection: a) Solution–average output, $\mathcal{S}_1$, b) Boundary output, $\mathcal{S}_2$.

In order to introduce the stabilized weak formulation of this problem [7, 8] we define

$$\begin{aligned} (w,v) &= \int_\Omega wv\,d\mathbf{x}, \qquad \langle w,v\rangle = \int_{\partial\Omega} \mathbf{U}\cdot\mathbf{n}\,wv\,ds,\\ \langle w,v\rangle_i &= \int_{\partial\Omega_i} \mathbf{U}\cdot\mathbf{n}\,wv\,ds, \quad \langle w,v\rangle_o = \langle w,v\rangle - \langle w,v\rangle_i. \end{aligned} \tag{3.2}$$

The coarse–mesh ($\delta = h$) and fine–mesh ($\delta = H$) forms required in (2.2) and (2.3), respectively, can then be expressed as

$$\mathcal{A}_\delta(w,v) := (\mathbf{U}\cdot\nabla w + \sigma w - f,\, v + \tau_{T_\delta}\mathbf{U}\cdot\nabla v) - (1+\tau_{T_\delta}\sigma)\langle w-g, v\rangle_i. \tag{3.3}$$

Note that, since the boundary conditions are imposed naturally, the functions in Y_H and Y_h are, in this case, unrestricted on the boundary.

The stabilization parameter τ_{T_δ} [7, 8] is taken to be constant over each triangle $T_\delta \in \mathcal{T}_\delta$: in $I\!R^1$,

$$\tau_{T_\delta} = |(\mathbf{l}_{12}\cdot\mathbf{l}_{12})/(2\mathbf{l}_{12}\cdot\bar{\mathbf{U}})| \tag{3.4}$$

while in $I\!R^2$,

$$\tau_{T_\delta} = [|(\mathbf{l}_{12}\cdot\bar{\mathbf{U}})/(\mathbf{l}_{12}\cdot\mathbf{l}_{12})| + |(\mathbf{l}_{23}\cdot\bar{\mathbf{U}})/(\mathbf{l}_{23}\cdot\mathbf{l}_{23})| + |(\mathbf{l}_{31}\cdot\bar{\mathbf{U}})/(\mathbf{l}_{31}\cdot\mathbf{l}_{31})|]^{-1}. \tag{3.5}$$

Here $\bar{\mathbf{U}}$ is the average value of $\mathbf{U}$ in the element, and $\mathbf{l}_{ij} = \mathbf{x}_j - \mathbf{x}_i$, where $\mathbf{x}_i$ and $\mathbf{x}_j$ are the coordinates of the element nodes i and j respectively. *A priori* error analysis of the resulting scheme [8] predicts an optimal convergence rate for the L_2–norm of error in the $\mathbf{U}$–directional derivative, $\|\mathbf{U}\cdot\nabla(u-u_h)\|_0 \le C\delta\|u\|_2$, and a near–optimal convergence rate for the L_2–norm of the error in the solution, $\|u-u_h\|_0 \le C\delta^{3/2}\|u\|_2$. Here $\|\cdot\|_r$ denotes the usual Sobolev norms [1].

It follows from the general formulation of Section 2.2 that $F = G = 0$ (and thus we set $\alpha = \beta = 0$), and that

$$E(w,v) := (\mathbf{U}\cdot\nabla w + \sigma w,\, v + \tau_{T_h}\mathbf{U}\cdot\nabla v) - (1+\tau_{T_h}\sigma)\langle w,v\rangle_i, \tag{3.6}$$

$$E^s(w,v) := (\mathbf{U}\cdot\nabla w,\, \tau_{T_h}\mathbf{U}\cdot\nabla v) + \sigma(w,v) + \frac{1+\tau_{T_h}\sigma}{2}[\langle w,v\rangle_o - \langle w,v\rangle_i]. \tag{3.7}$$

(We assume throughout this presentation that either $\sigma = 0$ or τ_{T_δ} is constant over all elements; the more general case gives rise to internal edge terms in (3.7) that, for simplicity, we do not include here.) Since E^s is positive semi–definite, we choose $E^s_Y := E^s$ (and hence $\gamma = 0$). We shall consider only linear outputs ($M = N = 0$) which can be expressed in the form

$$L(v) = (f^O, v) + \langle g^O, v\rangle_o, \tag{3.8}$$

where f^O and g^O are functions defined over Ω and $\partial\Omega_o$ respectively.

It remains only to specify the adjoint and hybrid fluxes. Towards that end, we define $\psi_H \in Y_H$ such that

$$E_H(v, \psi_H) = -[(f^O, v - \tau_{T_H}\mathbf{U}\cdot\nabla v) + (1 + \tau_{T_H}\sigma)\langle g^O, v\rangle_o], \quad \forall v \in Y_H, \tag{3.9}$$

where

$$E_H(w, v) := (\mathbf{U}\cdot\nabla w + \sigma w,\ v + \tau_{T_H}\mathbf{U}\cdot\nabla v) - (1 + \tau_{T_H}\sigma)\langle w, v\rangle_i. \tag{3.10}$$

Application of integration by parts (again assuming $\sigma = 0$ or τ_{T_H} uniform) yields the equivalent system

$$(v - \tau_{T_H}\mathbf{U}\cdot\nabla v,\ -\mathbf{U}\cdot\nabla\psi_H + \sigma\psi_H + f^O) + (1 + \tau_{T_H}\sigma)\langle v, \psi_H + g^O\rangle_o = 0, \quad \forall v \in Y_H, \tag{3.11}$$

which is clearly a stabilized coarse–mesh approximation of the adjoint problem

$$-\mathbf{U}\cdot\nabla\psi + \sigma\psi = -f^O \quad \text{in } \Omega, \tag{3.12a}$$

$$\psi = -g^O \quad \text{on } \partial\Omega_o. \tag{3.12b}$$

Note that the perturbation of the right hand side of equation (3.9) is necessary to obtain a consistent higher–order approximation to the continuous adjoint problem (3.12); inattention to this detail yields a much less accurate adjoint ψ_H.

Finally, the coarse–mesh hybrid fluxes can be calculated by solving the following *equilibration* problem [9, 2, 15, 16]: find $p^u_H \in Q_H$ and $p^\psi_H \in Q_H$ such that

$$b_H(v, p^u_H) = R^u_H(v), \quad \forall v \in \hat{Y}_H, \qquad b_H(v, p^\psi_H) = R^\psi_H(v), \quad \forall v \in \hat{Y}_H, \tag{3.13}$$

where $R^u_H(v) := -\mathcal{A}_H(u_H, v)$ and

$$R^\psi_H(v) := -[(f^O, v - \tau_{T_H}\mathbf{U}\cdot\nabla v) + (1 + \tau_{T_H}\sigma)\langle g^O, v\rangle_o] - E_H(v, \psi_H). \tag{3.14}$$

Here b_δ is the $(1+\tau_{T_H}\sigma)$ weighted sum over the edges of $\mathcal{T}_H$ of the product of q and the jump in v (trace of v on $\partial\Omega$); the $(1 + \tau_{T_H}\sigma)$ prefactor is included for consistency. It can be shown that (3.13) is solvable, thanks to equilibrium of u_H in (2.2) and of ψ_H in (3.9). (Note that, in the case in which $\mathcal{A}_H = \mathcal{A}_h = \mathcal{A}$, the bound procedure is considerably simpler to describe, and the interpretation of the adjoint and hybrid fluxes is much more transparent; the reader is refered to [18, 11, 10].)

We can now apply our general procedure; note that, due to the construction of the hybrid fluxes, (2.8) will be solvable even for $\sigma = 0$. For this particular application, $\mathcal{H}^-_{\alpha\beta\gamma} = \mathcal{H}^+_{\alpha\beta\gamma} = E^s$, $\hat{e}^u_- = \hat{e}^u_+ = \hat{e}^u$, $\hat{e}^\psi_- = \hat{e}^\psi_+ = \hat{e}^\psi$, and $\kappa^*_L = \kappa^*_U = \kappa^*$; the optimized bounds of equation (2.16) are thus computed as

$$s_- = \mathcal{S}(u_H) - 2E^s(\hat{e}^u, \hat{e}^\psi) - 2\sqrt{E^s(\hat{e}^u, \hat{e}^u)E^s(\hat{e}^\psi, \hat{e}^\psi)} - R^u(\psi_H), \tag{3.15a}$$

$$s_+ = \mathcal{S}(u_H) - 2E^s(\hat{e}^u, \hat{e}^\psi) + 2\sqrt{E^s(\hat{e}^u, \hat{e}^u)E^s(\hat{e}^\psi, \hat{e}^\psi)} - R^u(\psi_H). \tag{3.15b}$$

Furthermore (2.14) now reduces to

$$s_- = \mathcal{S}(u_h) - \kappa^* E^s(e - \hat{e}^{\kappa^*}_-, e - \hat{e}^{\kappa^*}_-), \tag{3.16a}$$

$$s_+ = \mathcal{S}(u_h) + \kappa^* E^s(e - \hat{e}^{\kappa^*}_+, e - \hat{e}^{\kappa^*}_+), \tag{3.16b}$$

for $\kappa^* = \sqrt{E^s(\hat{e}^\psi, \hat{e}^\psi)/E^s(\hat{e}^u, \hat{e}^u)}$ and $\hat{e}^{\kappa^*}_\pm = \hat{e}^u \mp \frac{1}{\kappa^*}\hat{e}^\psi$. It is clear from (3.16) that s_- (respectively s_+) is indeed a lower (respectively upper) bound for $\mathcal{S}(u_h)$ for all H.

3.1.2 One–Dimensional Example

We consider first a very simple one–dimensional numerical example in $\Omega :=]0,1[$, with $U_1 = 1$, $\sigma = 1$, $g = 0$, and f given by

$$f = \begin{cases} 1 - 3x, & \text{for } 0 < x \leq 0.5 \\ 2.5(x - 0.7), & \text{for } 0.5 < x \leq 0.7 \\ 0, & \text{for } 0.7 < x \leq 1 \end{cases} . \tag{3.17}$$

We consider only uniform meshes: the fine mesh is given by $h = 1/2560$, while the coarse mesh varies from $H = 1/10$ to $H = h$.

The first output considered, $\mathcal{S}_1$, is the integral of u over Ω, corresponding to $f^O := 1$ and $g^O := 0$ in (3.8). For each of the coarse meshes we compute the lower and upper bounds according to (3.15). The results are presented in Fig. 1a) in the form of $s_-/\mathcal{S}_1(u_h)$ and $s_+/\mathcal{S}_1(u_h)$; a convergence rate of $O(H^2)$ is observed. The second output considered, $\mathcal{S}_2$, is the value of u at $x = 1$, $u(1)$, corresponding to $f^O := 0$ and $g^O := 1$ in (3.8). The results are shown in Fig. 1b); in this case the observed convergence rate is $O(H^3)$.

3.1.3 Two–Dimensional Example

We consider the numerical solution of the two–dimensional convection equation on a unit square $\Omega :=]0,1[^2$. The convection velocity $\mathbf{U}$, is given by $\mathbf{U} := (-x_2, x_1)$; we take $\sigma = 0$ and $f = 0$. At the inflow boundary $\partial\Omega_i$, g is given by

$$g = \begin{cases} 5.0(x_1 - 0.2), & \text{for } 0.2 < x_1 \leq 0.4, \quad x_2 = 0 \\ 1, & \text{for } 0.4 < x_1 \leq 0.6, \quad x_2 = 0 \\ 1 - 5(x_1 - 0.6), & \text{for } 0.6 < x_1 \leq 0.8, \quad x_2 = 0 \\ 0, & \text{otherwise} \end{cases} . \tag{3.18}$$

The output considered is the weighted integral of the solution on the outflow boundary $\partial\Omega_i$, that is, $f^O = 0$ and

$$g^O = \begin{cases} 10(x_1 - 0.6), & \text{for } 0.6 < x_2 \leq 0.7, \quad x_1 = 0 \\ 1 - 10(x_1 - 0.7), & \text{for } 0.7 < x_2 \leq 0.8, \quad x_1 = 0 \\ 0, & \text{otherwise} \end{cases} . \tag{3.19}$$

The computational domain, together with the functions g and g^O, is sketched in Fig. 2.

A nearly uniform initial mesh consisting of 240 triangles is uniformly refined four times to generate a sequence of meshes with $240 \cdot 4^r$ elements for $r = 1, 2, 3$, and 4. The finest mesh so obtained, consisting of 61,440 triangles, is taken to be the fine mesh $\mathcal{T}_h$. For each of the coarser meshes we calculate the upper and lower bounds; the results are shown in Fig. 3. The observed convergence rate is slightly greater than $O(H^2)$, but certainly less than the convergence rate observed for the boundary output in the one–dimensional example.

We next implement the adaptive procedure described in Section 2.3.4. The starting triangulation is the coarsest mesh considered above, which has 240 triangles. On this mesh the error, given by Δ/s_{pre}, is 1.08. In the subsequent adaptive process all those triangles whose contribution to the bound gap is larger than 0.2 that of the largest elemental contribution are refined; the strategy described in [18] is used in order to treat the "hanging nodes" generated during the refinement process. The accuracy goal for Δ/s_{pre} is set to 0.001; a total of 10 meshes are generated before this goal is achieved. The final adapted mesh has 7,791 elements, which compares favourably with the uniform mesh that would be required to obtain a similar level of accuracy. In particular, a three–level uniformly refined mesh has 15,360 triangles, but

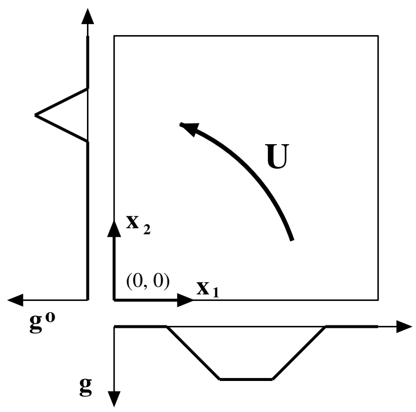

Figure 2: Two–dimensional linear convection: computational domain with the definition of the functions g and g^O.

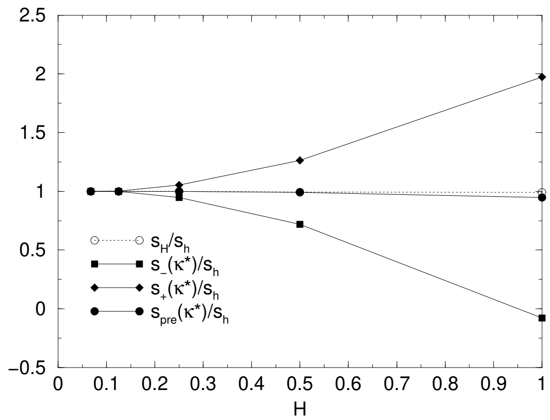

Figure 3: Two–dimensional linear convection: computed upper and lower bounds as a function of H.

only produces an accuracy $\Delta/s_{pre} = 0.002$. Fig. 4 shows the mesh and the contours for the computed solution u_H and adjoint ψ_H, initially, after one intermediate refinement step, and at the end of the adaptive process; note the effect of the adjoint (and hence output) structure on the mesh. Finally, Fig. 5 presents $2\Delta/s_{pre}$ as a function of the number of elements in $\mathcal{T}_H$ for both adaptive and uniform refinement.

3.2 The Burgers Equation

We consider now the Burgers equation [17], a one-dimensional nonlinear convection–diffusion equation. In particular we look for u such that

$$-\nu u_{xx} + \frac{1}{2}(u^2)_x = 0 \quad \text{in} \quad \Omega :=]0, 1[, \tag{3.20}$$

with Dirichlet boundary conditions $u(0) = 1$, $u(1) = 0$; the viscosity parameter ν is a real positive constant. The variational form of this problem is: find $u \in H^1_E(\Omega)$ such that

$$\nu(u_x, v_x, 1) - \frac{1}{2}(u, u, v_x) = 0, \quad \forall v \in Y, \tag{3.21}$$

where

$$(w, v, \omega) = \int_0^1 wv\omega \, dx. \tag{3.22}$$

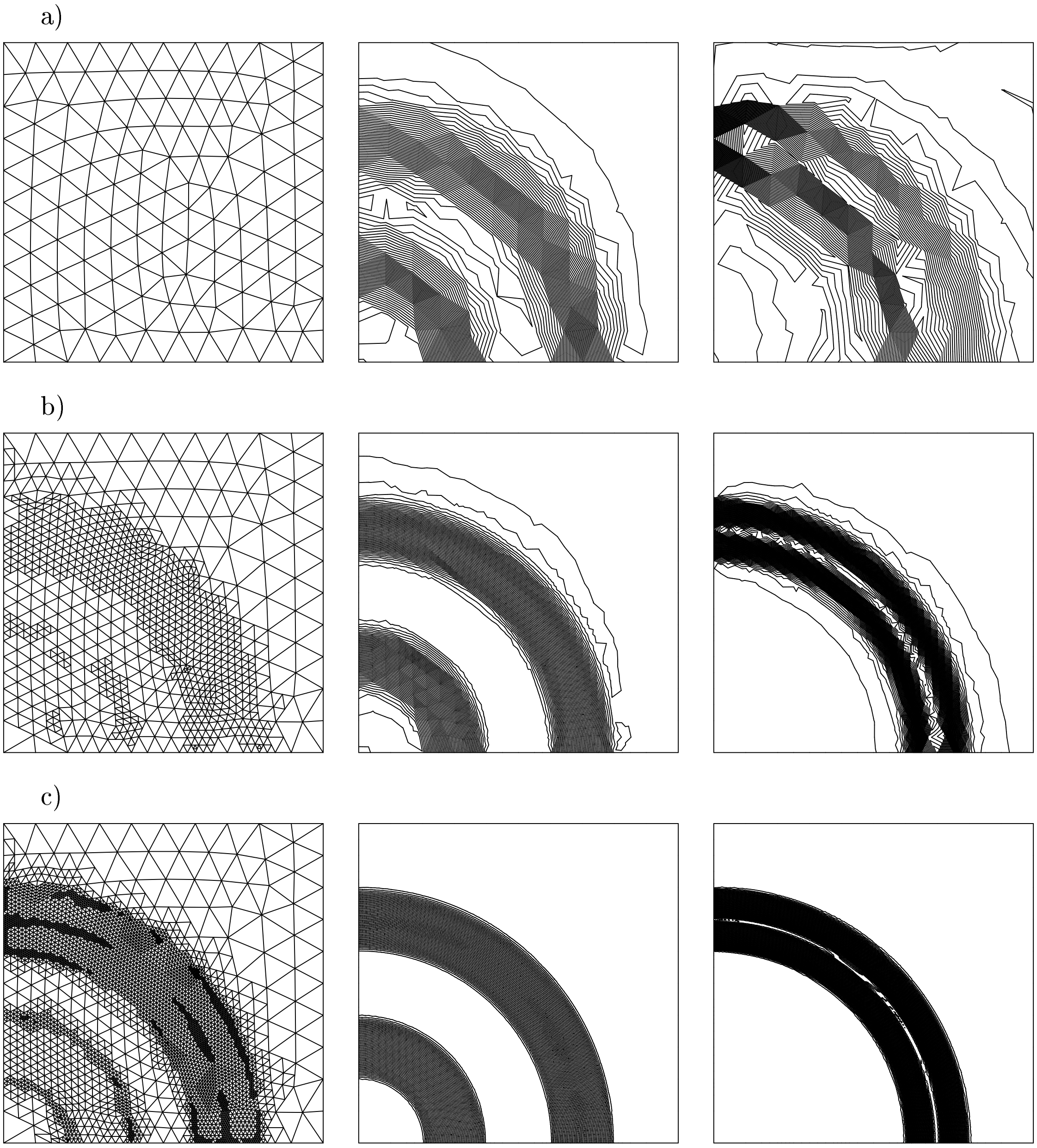

Figure 4: Two–dimensional linear convection: adaptively generated mesh (left), u_H (middle), and ψ_H (right), for a) the initial mesh of 240 elements and relative bound gap 108%, b) an intermediate mesh, after 5 refinements, of 1, 557 elements and relative bound gap 7.10%, and c) the final mesh, after 10 refinements, of 7, 791 elements and relative bound gap 0.1%.

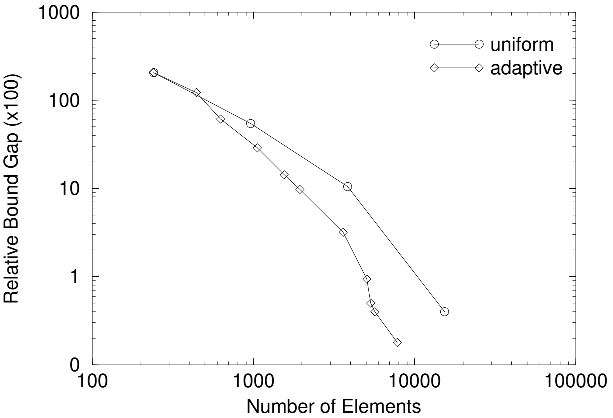

Figure 5: Two–dimensional linear convection: bound gap $2\Delta/s_{pre}$ as a function of the number of elements in $\mathcal{T}_H$ for meshes generated using uniform and adaptive refinement.

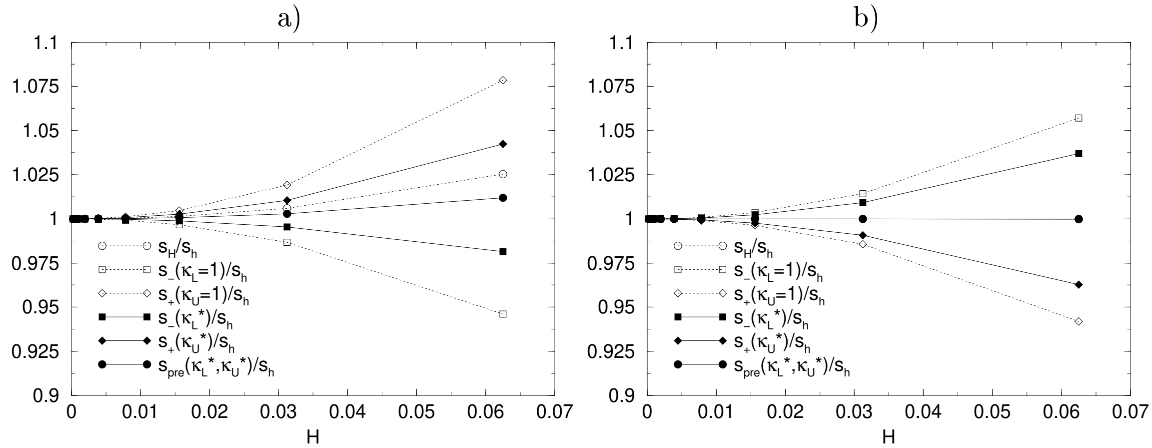

Figure 6: Burgers equation: a) Pointwise–value output, $\mathcal{S}_1$, b) Stress output, $\mathcal{S}_2$.

Here $H^1_E(\Omega)$ is the set of functions $v \in H^1(\Omega)$ [1] such that $v(0) = 1$, $v(1) = 0$; and Y is thus $H^1_0(\Omega)$, the space of functions in $H^1(\Omega)$ for which $v(0) = v(1) = 0$.

This problem can be readily cast in our general framework. In particular, we identify

$$\mathcal{A}(w, v) = \nu(w_x, v_x, 1) - \frac{1}{2}(w, w, v_x), \tag{3.23}$$

and then

$$\begin{aligned} E(w, v) &= \nu(w_x, v_x, 1) - (w, u_H, v_x), && (3.24)\\ E^s_Y(w, v) &= \nu(w_x, v_x, 1), && (3.25)\\ E^s_0(w, v) &= \frac{1}{2}(w, v, (u_H)_x), && (3.26)\\ F(w_1, w_2, v) &= -\frac{1}{2}(w_1, w_2, v_x). && (3.27) \end{aligned}$$

Note that $G(w, v) = 0$; also $\mathcal{A}_h = \mathcal{A}_H = \mathcal{A}$, as we apply no stabilization.

We consider two different outputs. For the first output we take the value of the solution u at a given point $\bar{x} \in]0, 1[$, $\mathcal{S}_1(u) = u(\bar{x})$, for which $L_1(v) = v(\bar{x})$, and $M_1(w_1, w_2) = N_1(w) = 0$. For the second output, $\mathcal{S}_2(u)$, we take the stress at $x = 1$, which we express as a nonlinear functional: we choose a $\chi \in C^0(\Omega)$ such that $\chi(0) = 0$ and $\chi(1) = 1$, and evaluate

$$\mathcal{S}_2(u) = \nu(u_x, \chi_x, 1) - \frac{1}{2}(u, u, \chi_x); \tag{3.28}$$

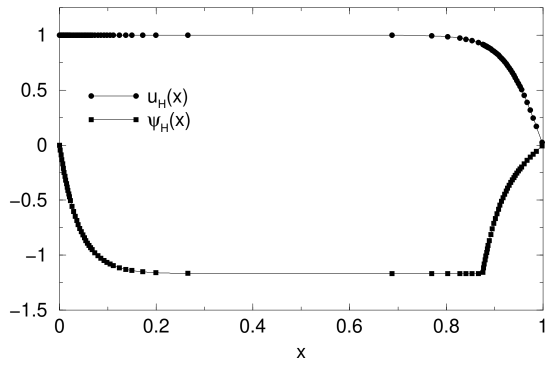

Figure 7: Burgers equation: adaptive solution and adjoint for output $\mathcal{S}_1$.

clearly, for u sufficiently smooth, we obtain $\mathcal{S}_2(u) = \nu u_x(1)$, as desired. In this case we identify

$$L_2(w) = \nu(w_x, \chi_x, 1) - (w, u_H, \chi_x), \tag{3.29}$$

$$M_2(w_1, w_2) = -\frac{1}{2}(w_1, w_2, \chi_x), \tag{3.30}$$

and $N_2(w) = 0$.

Finally, we must specify the adjoint and hybrid flux problems more precisely [17]; note that for this one dimensional problem, the hybrid fluxes reduce to scalars at the nodes of the coarse "triangulation." The adjoint satisfies

$$E(v, \psi_H) = -L(v), \quad \forall v \in Y_H; \tag{3.31}$$

the hybrid fluxes satisfy

$$b(v, p_H^u) = R^u(v), \quad \forall v \in \hat{Y}_H, \qquad b(v, p_H^\psi) = R^\psi(v), \quad \forall v \in \hat{Y}_H, \tag{3.32}$$

where $b(v, q)$ is the sum over all the nodes of $\mathcal{T}_H$ of the product of q and the jumps in v (save at $x = 0$, $x = 1$, where the "jump" is simply the trace of v). It is readily shown that (3.32) is solvable thanks to equlibrium of u_H in (2.2) and of ψ_H in (3.31). We can now directly apply the bound framework of Section 2.

For these definitions it can readily be shown, for instance for the more complex second output and $\alpha = \beta = \gamma = 1$, that, (say) (2.14a) reduces to

$$\begin{aligned} s_- &= \mathcal{S}(u_h) - \kappa_L \nu \int_0^1 (e - \hat{e}_-^{\kappa_L})_x^2 \, dx + \frac{\kappa_L}{2} \int_0^1 (e - \hat{e}_-^{\kappa_L})^2 (\psi_H + \chi - u_H)_x \, dx \\ &+ \frac{1 - \kappa_L}{2} \int_0^1 e^2 (\psi_H + \chi)_x \, dx; \end{aligned} \tag{3.33}$$

note that $F(e, e, e) = 0$. It is clear that the leading order deviation of s_- from $\mathcal{S}(u_h)$ is strictly negative; the remaining (indefinite) terms appear undifferentiated, and will thus be subdominant for H sufficiently small. It follows that s_- approaches $\mathcal{S}(u_h)$ from below — we obtain asymptotic bounds. The small prefactor ν may appear unhelpful in this regard, however the relevant quantity is, in fact, the *discrete* singular perturbation parameter — the grid Reynolds number. It follows that, as soon as the solution structure is even roughly resolved, bounds will obtain.

We now turn to the numerical experiments. We set $\nu = 0.04$, $\bar{x} = 0.875$, and $\alpha = \beta = \gamma = 1$; other values for the algorithm parameters are possible, and perhaps even preferred. We first consider the non-adaptive case with uniform meshes: the truth mesh is defined by $h = 1/8192$, and the coarse mesh by $H = 1/16$ (at the coarsest) to $H = h$ (at the finest). Figs 6a) and 6b) show the convergence of the bounds for output $\mathcal{S}_1$ and output $\mathcal{S}_2$, respectively; for both cases bounds are obtained for all H, and the measured rate of convergence is $O(H^2)$. The results obtained with the parameters $\kappa_L = \kappa_L^*$, $\kappa_U = \kappa_U^*$, are roughly twice as sharp as those with $\kappa_L = \kappa_U = 1$.

We next present results for the adaptivity algorithm described in Section 2.3.4; we consider output $\mathcal{S}_1$, and an accuracy goal of $\Delta/s_{pre} = 10^{-6}$. Fig. 7 shows the solution u_H and the adjoint ψ_H obtained after adaptive refinement. The final number of elements is $1,093$; in Fig. 7 the number of circles or squares in an interval is proportional to the concentration of elements (a square or circle for every 12 elements). Two zones of refinement can be identified: one for the "original" boundary layer in the solution, the other for the boundary layer that appears in the adjoint. There is a very clear advantage in this case to adaptive refinement.

Acknowledgements

This work was supported by NASA Grants NAG1-1978, NAG1-1587 and NAG4-105, DARPA and ONR Grant N00014-91-J-1889, and AFSOR Grant F49620-97-1-0052. L.M. is partially supported by Fulbright and BAEF Fellowships.

References

[1] R.A. Adams, *Sobolev Spaces*, Academic Press, New York, 1975.

[2] M. Ainsworth and J.T. Oden, *A unified approach to a posteriori error estimation using element residual methods*, Numer. Math., 65 (1993), pp. 23-50.

[3] M. Ainsworth and J.T. Oden, *A posteriori error estimation in finite element analysis*, Comp. Meth. in Appl. Mech. and Engrg., 142, (1997), pp. 1–88.

[4] R.E. Bank and A. Weiser, *Some a posteriori error estimators for elliptic partial differential equations*, Math. Comp., 44:170 (1985), pp. 283–301.

[5] R. Becker and R. Rannacher, *Weighted a posteriori error control in finite element methods*, IWR Preprint 96–1 (SFB 359), Heidelberg, 1996.

[6] R. Becker and R. Rannacher, *A feedback approach to error control in finite element methods: basic analysis and examples*, IWR Preprint 96–52 (SFB 359), Heidelberg, 1996.

[7] T.J.R. Hughes and M. Mallet, *A New Finite Element Formulation for Computational Fluid Dynamics : III. The Generalized Streamline Operator for Multidimensional Advective–Diffusive Systems*, Comp. Meth. in Appl. Mech. and Engrg., 58 (1986), pp. 305-328.

[8] C. Johnson, U. Nävert and J. Pitkäranta, *Finite Element Methods for Linear Hyperbolic Problems*, Comp. Meth. in Appl. Mech. and Engrg., 45 (1984), pp. 285–312.

[9] P. Ladeveze and D. Leguillon, *Error estimation procedures in the finite element method and applications*, SIAM J. Numer. Anal., 20 (1983), pp. 485–509.

[10] Y. Maday, A.T. Patera and J. Peraire, *A general formulation for a posteriori bounds for output functionals of partial differential equations; application to the eigenvalue problem*, submitted to C.R. Acad. Sci. Paris, March 1998.

[11] Y. Maday and A.T. Patera, *Numerical analysis of a posteriori finite element bounds for linear–functional outputs,* Mathematical Models and Methods in Applied Science, submitted.

[12] M. Paraschivoiu, *A posteriori finite element bounds for linear-functional outputs of coercive partial differential equations and of the Stokes problem*, PhD thesis, Department of Mechanical Engineering, Massachusetts Institute of Technology 1997.

[13] M. Paraschivoiu and A.T. Patera, *A hierarchical duality approach to bounds for the outputs of partial differential equations*, Comp. Meth. in Appl. Mech. and Engrg., to appear.

[14] M. Paraschivoiu and A.T. Patera, *A posteriori bounds for linear–functional outputs of Crouzeix–Raviart finite element discretizations of the incompressible Stokes problem*, Int. J. for Num. in Fluids, submitted.

[15] M. Paraschivoiu, J. Peraire, and A.T. Patera, *A posteriori finite element bounds for linear-functional outputs of elliptic partial differential equations*, Comp. Meth. in Appl. Mech. and Engrg., 150 (1997), pp. 289–312.

[16] M. Paraschivoiu, J. Peraire, Y. Maday, and A.T. Patera, *Fast bounds for outputs of partial differential equations*, in Proceedings of the Workshop on Optimal Design and Control, J. A. Burns, E. M. Cliff, and B. Grossman, eds., Progress in Systems and Control Theory, Birkhäuser, 1998.

[17] J. Peraire and A.T. Patera, *Asymptotic a posteriori finite element bounds for the outputs of noncoercive problems: the Helmholtz and Burgers equations* (Tech. Rep. 97-12-1, MIT Fluid Mechanics Laboratory, December 1997), Comp. Meth. in Appl. Mech. and Engrg., submitted.

[18] J. Peraire and A.T. Patera, *Bounds for linear-functional outputs of coercive partial differential equations: Local indicators and adaptive refinement*, in On New Advances in Adaptive Computational Methods in Mechanics, P. Ladeveze and J. T. Oden, eds., September 1997.

[19] R. Rannacher and F.-T. Suttmeier, *A feedback approach to error control in finite element methods: application to linear elasticity*, Preprint 96–42 (SFB 359), Heidelberg, 1996.

[20] R. Verfürth, *A Review of a Posteriori Error Estimates and Adaptive Mesh–Refinement Techniques*, Wiley–Teubner, 1997.